Electronic Supplementary Material (ESI) for Nanoscale.

Thermo-Electro-Optical Properties of Seamless Metallic Nanowire Networks For Transparent Conductor Applications

K. Esteki[1], D. Curic[1], H. G. Manning[2,3], E. Sheerin[2,3], M. S. Ferreira[3,4], J. J. Boland[2,3], and C. G. Rocha[1,5,6*]

[1]Department of Physics and Astronomy, University of Calgary, 2500 University Drive NW, Calgary, Alberta T2N 1N4, Canada
[2]School of Chemistry, Trinity College Dublin, Dublin 2, Ireland
[3]Advanced Materials and Bioengineering Research (AMBER) Centre, Trinity College Dublin, Dublin 2, Ireland
[4]School of Physics, Trinity College Dublin, Dublin 2, Ireland
[5]Hotchkiss Brain Institute, University of Calgary, 3330 Hospital Drive NW, Calgary, Alberta T2N 4N1, Canada
[6]Institute for Quantum Science and Technology, University of Calgary, Calgary, Alberta, Canada T2N 1N4

[*]Author to whom correspondence should be addressed: claudia.gomesdarocha@ucalgary.ca

1. Voronoi-based Nanowire Networks in COMSOL

This study used the finite element method (FEM) included in COMSOL Multiphysics® software to construct electrothermal modelling and the optical scattering characterisation of seamless NWNs. For the electrothermal modelling, an expanded 3D model of heat transfer in a seamless NWN composed of Ag, Au, Al, and Cu has been conducted. The thermal and electrical characteristics of the network systems are carried out employing the COMSOL Multiphysics package by integrating its “electric current” (EC) and “heat transfer in solid” (HT) modules; this is done so that the local temperature distribution patterns through the network and heterogeneous current density profiles can be better understood. The thermo-electrical equations solved for the seamless NWN are given in equation (2) of the main text. The 3D volume of the object was discretized using the COMSOL meshing module’s physics-controlled mesh refinement, which includes progressively changing the mesh size from coarse to fine. This method was used to

guarantee that the resulting mesh would be suitable for mapping spatial temperature variations as shown in Figure S1.

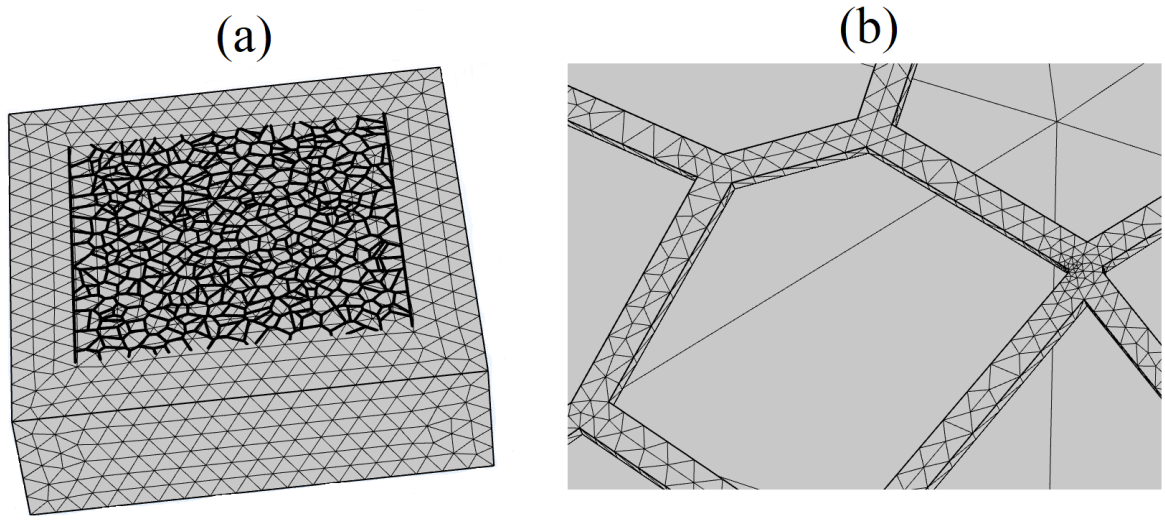

Figure S1. (a) Discretized meshing of a seamless NWN placed on a substrate. (b) Close-up of a seamless NWN taken from panel (a).

2. Wiedemann-Franz Law and Extra Thermal Analysis

In order to investigate the effect of Joule heating and to ultimately map the distribution of local current density and temperature gradient profiles in the seamless NWNs at variable bias voltages, we performed the thermal characterization in conjunction with the electrical characterization using the Wiedemann-Franz's relationship[1, 2] that relate electrical and thermal conductivity. The Wiedemann-Franz rule states that a metal's thermal conductivity (k_{cond}) is proportional to its temperature (T) in the form of $k_{cond}/\sigma = \mathcal{L}T$ in which $\mathcal{L}$ is the Lorenz number. In Figure S2, we compare the electrical conductivity of four different materials as a function of temperature, taken from the Wiedemann-Franz rule, revealing that the electrical conductivity of Ag is most sensitive to temperature change.

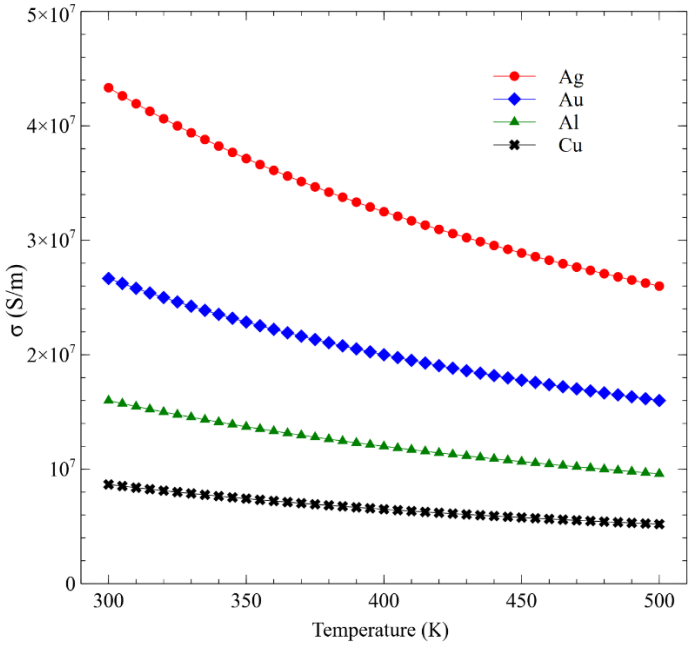

Figure S2. Wiedemann-Franz relationship plot for Ag, Au, Al, and Cu. The vertical axis depicts the temperature-dependent change in electrical conductivity, while the thermal conductivity remains constant to the values given on Table 1 in the main text.

The reported melting points of bulk Ag, Au, Al, and Cu are approximately reported to be 1234 K, 1336 K, 933 K, 1357 K, respectively[3], whereas those of individual nanowires are 873 K[4], 1300 K[5], 894 K[6], and 1073 K[7], respectively. The average maximum temperatures within the described geometric structure provided in this research for $AF = 0.08$ to $AF = 0.25$ and $AR = 0.1$ to $AR = 3.0$ are computed for all applied voltages and displayed in Figure S3. This calculation allows us to make estimations or comparisons between our calculated average temperature values with typical experimental melting points of nanoscale structures.

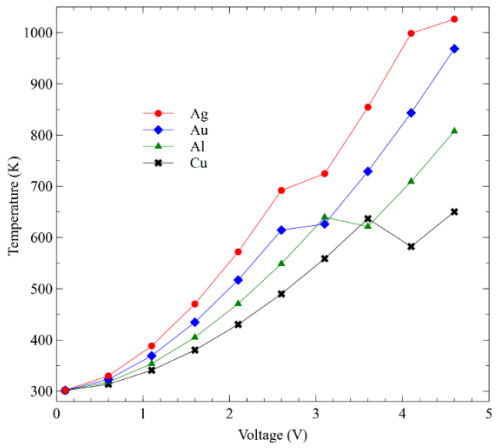

Figure S3. Average maximum temperatures as a function of bias voltage for seamless NWNs with geometrical features varying as $AF = 0.08$ to $AF = 0.25$ and $AR = 0.1$ to $AR = 3.0$. Each material is represented by their corresponding legend color and marker as for Ag by red/circle, Au by blue/diamond, Al by green/triangle, and Cu by black/cross.

3. Extra Optical Characterization

To numerically solve the Maxwell's equations in the frequency domain, a FEM analysis was created utilising the "electromagnetic waves" and "frequency domain" interfaces accessible in the "radio frequency" module in COMSOL. To simulate the electric field scattered from a nanoscale object, we set COMSOL to solve Maxwell's differential equations in a 2D space domain. Our primary COMSOL optical simulation output is the extinction efficiency coefficients, which are defined as $Q_{ext} = Q_{abs} + Q_{sca}$ with Q_{ext}, Q_{abs} and Q_{sca} being the extinction, absorption, and scattering coefficients, respectively. The seamless NWNs used for this analysis are built with a channel-like cross section, similar to a 2D rectangular shape with equal sides, rather than the more conventional circular cross-section for a cylinder. Our prior work[8] provides in-depth explanations of the COMSOL modelling setups, including elements such as the electromagnetic wave background, perfect electric conductors (PECs), scattering boundary conditions, object quantization into meshing, and the relevant Maxwell's electromagnetic wave equations that need

to be solved. In our previous study[8], we computed the optical spectra of a cylinder cross-section of a nanowire subjected to direct light incidence and compared the results with those derived from Mie light scattering theory (MLST)[9] for an infinite cylinder, providing independent confirmation of the optical COMSOL analysis performed in this study. The MLST[9] and our optical COMSOL simulation were found to be in excellent agreement. We therefore have extended the same COMSOL framework to model an object with a squared cross-sectional area. For nanochannels comprising a square cross-sectional area of sides $W = D = 30\,nm$ and $W = D = 50\,nm$, full-wave electromagnetic solutions were performed spanning the entire the wavelength range of 150 to $1200\,nm$ as depicted in Figure 5 of the main text.

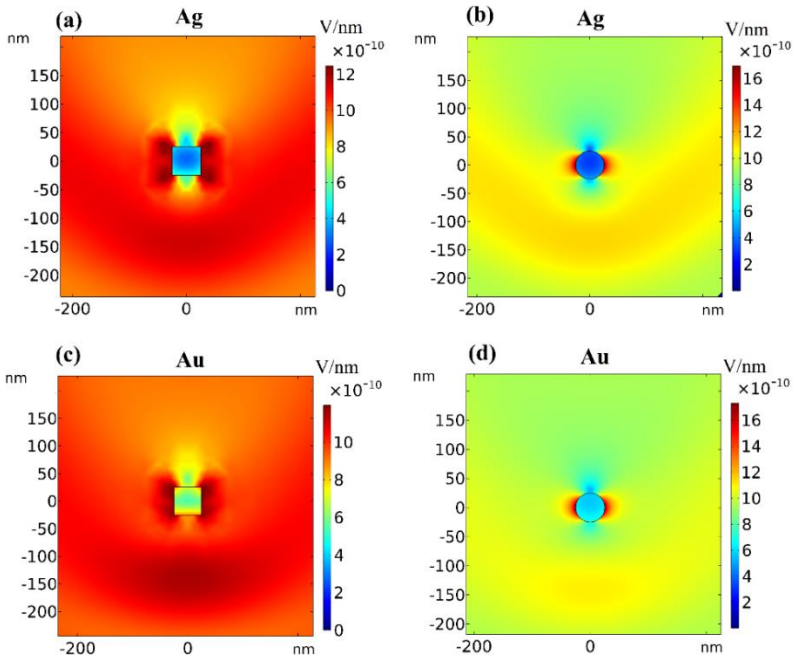

Figure S4. Electric field distribution in the vicinity of the square and cylinder cross-sections of a nanowire in the x-y plane. The nanowires are made of (a-b) silver and (c-d) gold, and their cross-sectional dimensions are, respectively, $D = W = 50\,nm$ and $d = 50\,nm$ for square and cylinder cross-sections. A plane wave with wavelength of $\lambda = 550\,nm$ along the y-axis orientation illuminates the square/circle geometries. There are two normal polarizations along the x- and z-axes of the geometry. The mean of the two perpendicular electric field polarizations is shown in the colour bar as the electric field intensity (V/nm).

The electric field strengths scattered off square/circular geometries are presented in Figures S4 and S5 for a seamless nanochannel with a square cross-section and a cylindrical nanowire with circular cross-section. Their material composition was also changed: Ag and Au (Figure S4); Al and Cu (Figure S5). The relative electric field intensities in the vicinity of a square cross-section nanochannel and a circular cross-section nanowire reveal an increase of about 1.2 for the squared structure. Al exhibits the strongest electrical field intensities overall compared to the other target materials tested here.

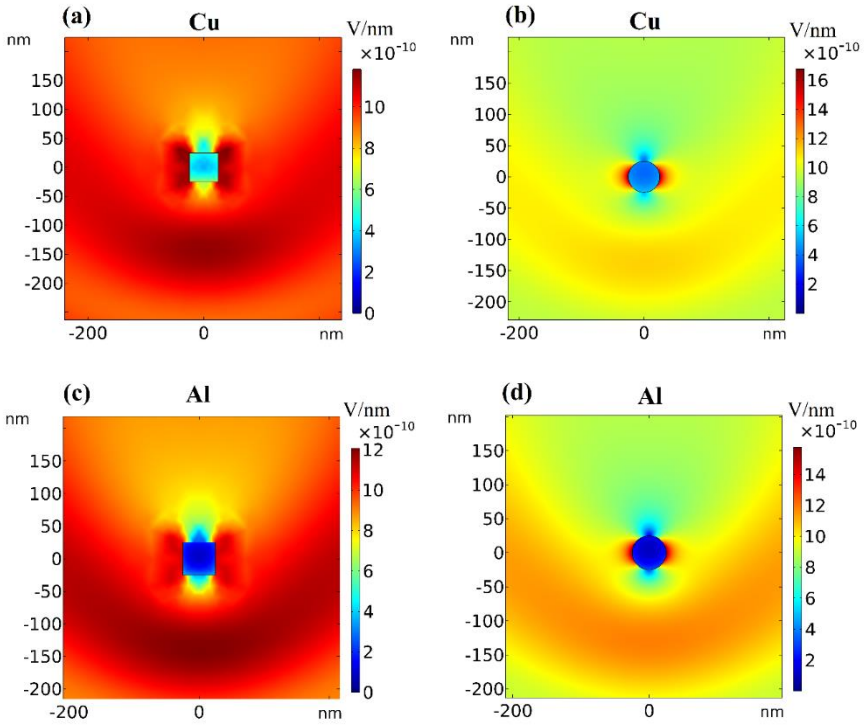

Figure S5. Electric field distribution in the vicinity of the square and cylinder cross-sections of a nanowire in the x-y plane. The nanowires are made of (a-b) copper and (c-d) aluminum, and their cross-sectional dimensions are, respectively, $D = W = 50\,nm$ and $d = 50\,nm$ for square and cylinder cross-sections. A plane wave with wavelength of $\lambda = 550\,nm$ along the y-axis orientation illuminates the square/circle geometries. There are two normal polarizations along the x- and z-axes of the geometry. The mean of the two perpendicular electric field polarizations is shown in the colour bar as the electric field intensity (V/nm).

4. Literature Direct Comparison

Table S1. Literature comparison of various physical quantities reported in various works, including experimental ones, and ours targeting transparent conductors/heaters made of NWNs. 'PS' stands for 'present study', 'N/A' stands for 'not applicable' which indicates there was no information found in the corresponding reference, 'Temp.' is the temperature, 'Ref.' stands for 'reference', and R_s is the sheet resistance.

Experimental Comparisons						
Material	**Width/Depth (μm)**	**Device Dimensions**	**Voltage (V)**	**Temp. (K)**	**R_s Ω/□**	**Ref.**
Ag[1]	55/0.08	2.5 × 2.5 cm^2	N/A	380	8	[10]
Ag[1]	N/A	5 × 5 cm^2	3-9	350	26.9-142	[11]
Ag[1]	100/125	4 × 2 cm^2	1-5	373	2-6	[12]
Ag[1]	2-9/1-5	2 × 2 cm^2	1-4	473	1.13	[13]
Ag[1]	21-70/0.3	10 × 8 cm^2	8.5	443	1	[14]
Au[1]	3–20/10	N/A	3-6	320-360	3-6	[15]
Au[1]	2-10/0.08	0.015 × 0.01 cm^2	0.7-1.5	373	1.5-10	[16]
Au[1]	0.5-2/0.06-0.22	2.5 × 2.5 cm^2	7-12	583-783	3.1-5.4	[17]
Al[2]	2-6/6.5	0.02 × 0.02 cm^2	4-14	323-573	3	[18]
Cu[3]	N/A/0.8	N/A	0.5-5	433	2-160	[19]
Ag[3]	Diameter-0.055	N/A	1-4	323-573	1-10	[20]
Ag[3]	250/0.2	1 × 1 cm^2	0.8	343	2-4	[21]
Ag[3]	7/1.12	0.03 × 0.01 cm^2	5	380	2-7	[22]
Au[3]	5/0.15	2 × 2 cm^2	5.5	434	1.5-5.5	[23]
Cu[4]	Diameter-0.25	5 × 5 cm^2	N/A	345	6.5	[24]
Cu[4]	Diameter-0.115	3.5 × 5 cm^2	N/A	333	1-124	[25]
Ag[1]	0.05-0.5/0.05-2	50 × 50 μm^2	0.5-4.6	470	1-19	PS.
Au[1]	0.05-0.5/0.05-2	50 × 50 μm^2	0.5-4.6	425	1-28	PS.
Al[1]	0.05-0.5/0.05-2	50 × 50 μm^2	0.5-4.6	390	1-42	PS.
Cu[1]	0.05-0.5/0.05-2	50 × 50 μm^2	0.5-4.6	350	1-80	PS.

[1] Seamless NWN
[2] Hybrid Seamless NWN
[3] Grid Mesh NWN
[4] Standard NWN

Table S1 contains a literature comparison of the electro-thermal properties of various NWN systems made of metallic materials (Ag, Au, Al, and Cu) fabricated with varied device dimensions and subjected to variable bias voltages. Note that all these works already deal with transparent conductors with sufficiently high optical transmissions ($\gtrsim 90\%$), as a result we did not include this information on this table. This comparison between previously published (experimental)

findings and the results of our simulations reveals a remarkable agreement, indicating the validity of our computational investigation. Although the electrothermal outcomes remain consistent with the experimental results, the reduced dimensions of our seamless NWNs suggest superior electrical and thermal conductivity, rendering them highly suitable for deployment as transparent electrodes. Some of the highlights on the table we would like to point out are:

- Our average temperatures obtained for seamless Cu NWNs agree with references 24 and 25 and are considerably lower when compared with the findings of reference 19. Nonetheless, the latter studied regular seamless Cu meshes in which temperature distributions can differ considerably in comparison to more disordered network frames as the Voronoi arrangement studied in our work.

- There is a wide range of average temperatures obtained for seamless Ag NWNs in the literature (see first five rows on the table). Our results agree with references 13 and 14 in which Voronoi-like Ag NWNs fabricated on insulating substrates were investigated experimentally. Other experimental setups result in temperature differences as for the case of reference 11 in which Ag NWNs were prepared as paper-based heaters. The thermal interaction of the NWN with distinct substrates can be modelled by altering the contact thermal conductance as we demonstrated in Figure 14 of the current manuscript. In that result, we demonstrated that it is possible to reduce the average temperature of Ag NWNs up to ~300 K by increasing the contact thermal conductance mediating the interaction between the network and substrate.

- In terms of sheet resistance values, due to the significant NWN size difference between the cited works on Table S1 and ours, their sheet resistance values tend to be relatively lower

than some of our estimations. Sheet resistance (R_s) values also depend significantly on the contact resistance (R_c) between the NWN and the electrodes that interrogate the sample electrically. This is an information that can be challenging to acquire, for this reason, in our simulations, we considered sufficiently good contacts between the NWN and the electrodes by setting R_c~1 Ω or $R_c \approx \langle R_{in} \rangle$ in which $\langle R_{in} \rangle$ is the average inner resistance of all nanowire segments in the Voronoi NWN. With exception of reference 11 which provides a wide range of sheet resistance values for Ag NWNs, our numerical predictions encompass the values of all selected works depicted on the table for seamless NWNs. We also included for the sake of reference, sheet resistance values for NWNs of other layouts than the Voronoi arrangement such as grid mesh NWNs and junction-based (standard) NWNs.

5. Supplemental Weibull Analysis in Seamless NWNs

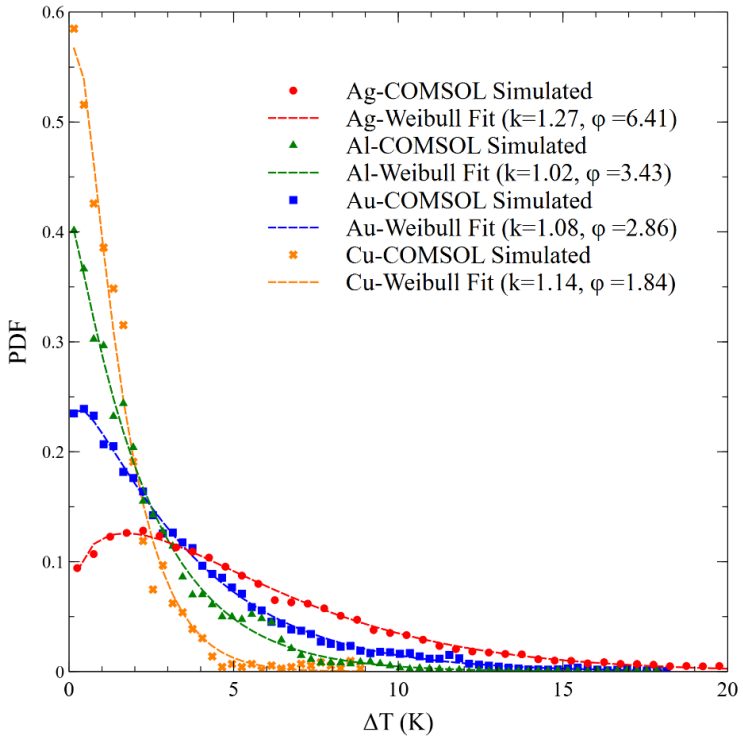

Figure S6. Temperature difference distributions obtained for seamless NWNs made of distinct metals, $AF = 0.185$ and $AR = 3$ and fixed bias voltage of 1.1 V. These were obtained using COMSOL Multiphysics set for electrothermal simulations. (Dashed lines) Fitting of Weibull probability density function (PDF) for each case study. The values of the fitting parameters are presented on legend.

Earlier research has documented the presence of a universal temperature profile in junction-based random NWNs, which can be accurately described using a two-parameter Weibull probability density function[26, 27]. Our calculations have shown that seamless metallic NWNs exhibit thermal transport properties that follow the Weibull distribution, making them another example of a network-based system with this statistical behavior. Electrothermal simulations using COMSOL Multiphysics were utilized to obtain temperature difference distributions for seamless NWNs composed of different metals, with a fixed voltage of 1.1 V and $AF = 0.185$ and $AR = 3$, and are shown in Figure S6.

To supplement this analysis in terms of Weibull temperature variation distributions, we conducted a COMSOL calculation for distinct metallic seamless NWNs, but their geometry was set "thicker" than the one set in Figures 16 (main manuscript) and Figure S6. This is to also have a case study to determine the effects of widening the thickness of the nanowire ridges on the temperature distributions. We obtained the temperature variation distribution in seamless NWNs of AF = 0.185 and AR = 2 (W = 0.26 μm and D = 0.132 μm) which is in fact made of wider ridges than the NWNs reported in Figure 16 (main manuscript) and Figure S6 with AR = 3 (W = 0.24 μm and D = 0.08 μm). In both cases, the network experiences a bias voltage of 4.6 V. This result is shown in Figure S7. All distributions shifted to higher temperatures indicating that the increase in the ridge thickness enables the networks to sustain higher temperatures, demonstrating that potential to failure can occur at higher temperature ranges. The Weibull fitting parameters indicate slight

fluctuations in the shape parameter k in comparison to the results in Figure 16, but all scale parameters ϕ increased as a result of this temperature shift. In terms of mean temperature change to failure for this new set of curves calculated with equation (5) in the main manuscript, we obtained:

$$\langle \Delta T \rangle_f (Ag) = 105.48\ K$$

$$\langle \Delta T \rangle_f (Au) = 76.78\ K$$

$$\langle \Delta T \rangle_f (Al) = 54.15\ K$$

$$\langle \Delta T \rangle_f (Cu) = 34.40\ K.$$

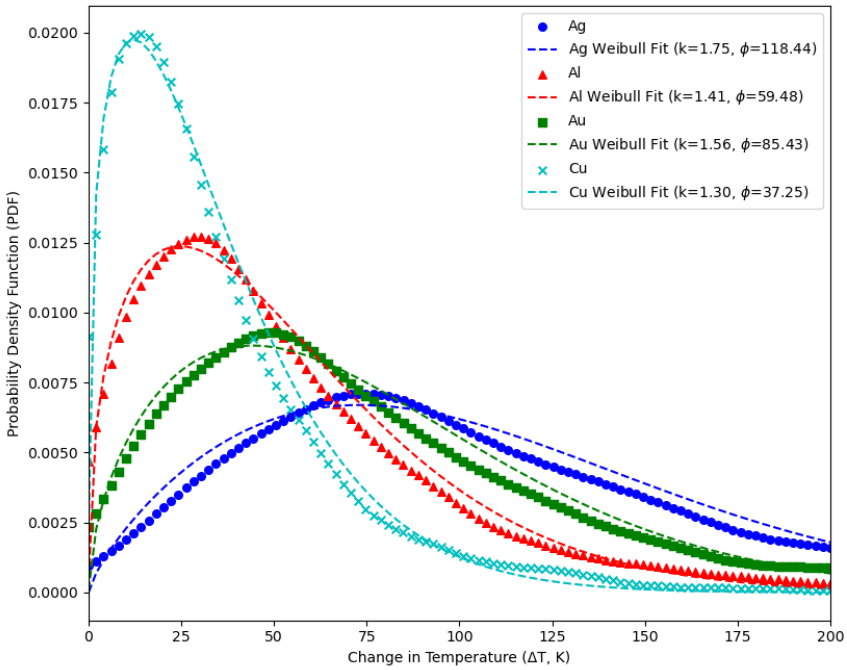

Figure S7: Temperature difference distributions obtained for seamless NWNs made of distinct metals, AF $= 0.185$ and AR $= 2$ and fixed bias voltage of 4.6 V. These were obtained using COMSOL Multiphysics set for electrothermal simulations. (Dashed lines) Fitting of Weibull probability density function (PDF) for each case study. The values of the fitting parameters are presented on legend.

6. Comparison and Model Validation

This section has the goal to demonstrate that our modelling approaches have been compared and validated from procedures tested in our past works and by comparisons with other theoretical works found in the literature. This serves as a way to support our computational framework with important validation arguments of our calculations which were put in place and are highlighted here for clarity.

Comparison #1)

Our current computational scheme used to obtain the sheet resistance of nanowire networks (NWNs) is the same as adopted in our previous work "Ultimate conductivity performance in metallic nanowire networks"[28]. In that work, we had numerical sheet resistances comparable with experimental sheet resistance values by adjusting the interwire junction resistances and the NWN densities. Our model predicted sheet resistances in the same order of magnitude as the experimental ones which ranged from 15-190 Ohms (see supplemental information of [28]) for Ag NWNs. Seamless NWNs are "junctionless" structures that can be described using the same network resistive scheme as in [28], however, the voltage nodal allocation will differ due to the lack of junctions. In this way, Voronoi-based NWNs are simpler to model since they have one less tunable parameter, in this case, the interwire junction resistances which can also be very experiment-dependent, and exhibit pronounced fluctuations due to dynamical atomistic events happening inside the wire-wire connections. The primary resistance contribution in seamless Voronoi-based NWNs is the inner resistances associated with each nanowire segment which can be calculated with precision given the material resistivity, the nanowire segment length, and its cross-sectional area. The latter three quantities are taken from experimental data, as a result, inner resistance predictions fall within expected experimental findings.

Comparison #2)

The numerical procedures used to compute the sheet resistance of NWNs used in this work were also contrasted with other analytical descriptions as we did in O'Callaghan et al. [29]. In that work, we compared our numerical resistive model with results obtained using analytical Green's functions and Effective Medium Theory (EMT) describing disordered and square lattice of resistors (see Figure 2 of that manuscript). The numerical results using Modified Nodal Analysis agree with the analytical EMT trends as that figure indicates.

Comparison #3)

Another important validation is included in Figure 9 of the current manuscript. There we directly compared the sheet resistance results coming from two very different computational methodologies: in-house scripts using Nodal Modified Analysis and COMSOL which is finite difference mesh-based. Although both methods are completely independent and have very different settings, their results agree very well for various aspect ratios and area fraction values.

Comparison #4)

Our optical extinction model was validated in our previous work in Esteki et al. [8] in which we compared our COMSOL model with the standard Mie Light Scattering Theory (MLST) as shown in Figure 2 of that paper. Within the MLST formalism, optical characteristics in nanomaterials are derived from the effective analytical solutions to Maxwell's equations, which take into account the scattering of electromagnetic radiation by the nanoparticles. Our COMSOL model was calibrated in accordance with MLST as the figure indicates and the same settings were transferred to the context of this study targeting seamless NWNs.

Comparison #5)

We conducted an extra analytical analysis to support the validation of our numerical calculations. Kumar et al. [30] developed an analytical approach using geometric reasoning and image analysis to provide a comprehensive understanding of the behaviour and properties of distinct conducting network structures, including standard NWNs and Voronoi-based ones. In their paper, they obtained an analytical prediction of sheet resistances in conductive networks as

$$\boldsymbol{R_s = \frac{\pi}{2}\frac{\rho_e}{wt\sqrt{n}}} \qquad \text{(Eq. S1)}$$

where R_s is the sheet resistance of the network, w is the width, t is the thickness (depth), n is the network density, and ρ_e is the electrical resistivity of the material. This equation indicates that the sheet resistance should scale with the square root of the NWN density. To prove that our numerical scheme also gives the same analytical trend, we created Figure S8 below which shows the sheet resistance calculated for ensembles of Voronoi NWNs of various densities using our numerical routines based on Modified Nodal Analysis. The blue dashed line is a fitting of the scaling law above confirming that our numerical procedure recovers the analytical prediction of $R_s \propto n^{-1/2}$ with the fitting parameter compacting information about the NWN thickness, width, and an effective electrical resistivity associated to the network material and its connectivity. The fitting of a $y = a\, n^{-1/2}$ curve onto the simulated data points gives a proportionality factor of $a = 17.42$ which corresponds to an effective resistivity of $\rho_e = 27.7\ n\Omega m$, and $w = t = 50\ nm$. Note that the material resistivity value used in the simulation that generated the data points is of $\rho_{sim} = 20\ n\Omega m$ and $w_{sim} = t_{sim} = 50\ nm$ but ρ_e taken from the fitting is expected to be higher than ρ_{sim} since the NWN is not simply a bulk cuboid solid material, it is a material with voids and disordered segments arranged in a Voronoi frame, resulting in a higher intrinsic resistivity.

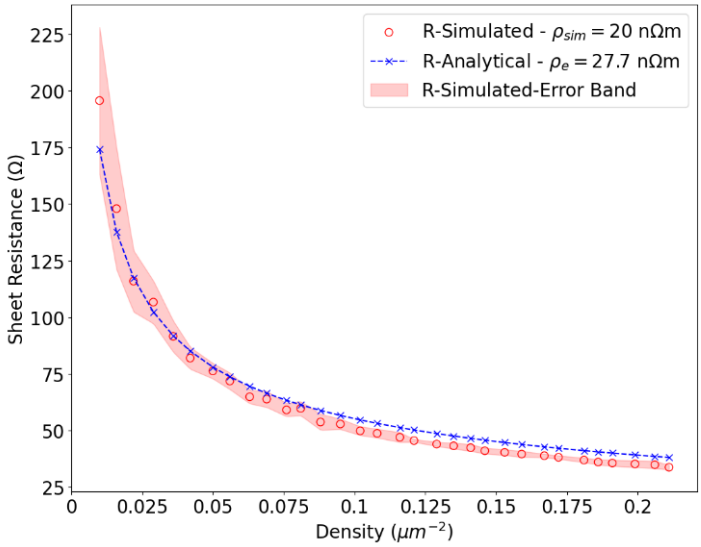

Figure S8: Comparison between calculated sheet resistances using numerical Modified Nodal Analysis (R-Simulated) and the analytical trend in equation S1 obtained for disordered Voronoi-based NWNs. R-Simulated is shown as red circles. The network dimension is $50 \times 50\ \mu m$. Each data point was obtained by averaging the results from 10 randomly generated spatial networks. The error band (shaded region) shown in the figure represents the standard deviation of the averaged ensembles. The parameters involved in the simulations are the electrical resistivity $\rho_{sim} = 20\ n\Omega m$, the width, and the thickness (depth) of the network $w_{sim} = t_{sim} = 50\ nm$. R-Analytical (crossed blue dashed line) is computed according to the equation S1 being fitted to the data points. From the fitting of $R_s = a\ n^{-1/2}$, $a = \pi\rho_e/2wt = 17.42$ from which $\rho_e = 27.7\ n\Omega m$ was found.

References

[1] Wang J, Wu Z, Mao C, Zhao Y, Yang J, Chen Y. Effect of electrical contact resistance on measurement of thermal conductivity and Wiedemann-Franz law for individual metallic nanowires. Scientific reports. 2018;8(1):1-8.

[2] Franz R, Wiedemann G. Ueber die Wärme-Leitungsfähigkeit der Metalle. Annalen der Physik. 1853;165(8):497-531.

[3] https://www.onlinemetals.com/en/melting-points. [Internet].

[4] Mayoral A, Allard LF, Ferrer D, Esparza R, Jose-Yacaman M. On the behavior of Ag nanowires under high temperature: in situ characterization by aberration-corrected STEM. Journal of Materials Chemistry. 2011;21(3):893-8.

[5] Huber SE, Warakulwit C, Limtrakul J, Tsukuda T, Probst M. Thermal stabilization of thin gold nanowires by surfactant-coating: a molecular dynamics study. Nanoscale. 2012;4(2):585-90.

[6] Davoodi J, Dadashi S, Yarifard M. Molecular dynamics simulations of the melting of Al–Ni nanowires. Philosophical Magazine. 2016;96(22):2300-10.

[7] Haase D, Hampel S, Leonhardt A, Thomas J, Mattern N, Büchner B. Facile one-step-synthesis of carbon wrapped copper nanowires by thermal decomposition of Copper (II)–acetylacetonate. Surface and Coatings Technology. 2007;201(22-23):9184-8.

[8] Esteki K, Manning H, Sheerin E, Ferreira M, Boland JJ, Rocha CG. Tuning the electro-optical properties of nanowire networks. Nanoscale. 2021;13:15369-79.

[9] Bohren CF, Huffman DR. Absorption and scattering of light by small particles: John Wiley & Sons; 2008.

[10] Zeng Z, Wang C, Gao J. Numerical simulation and optimization of metallic network for highly efficient transparent conductive films. Journal of Applied Physics. 2020;127(6):065104.

[11] Tao J, Li S, Shi J, Ji S. Enhancing the Optical Response Speed of Thermochromic Paper Displays by Heat Exchange Manipulation of Invisible Heaters. ACS Applied Energy Materials. 2023;6(5):2897-905.

[12] Gupta R, Rao K, Srivastava K, Kumar A, Kiruthika S, Kulkarni GU. Spray coating of crack templates for the fabrication of transparent conductors and heaters on flat and curved surfaces. ACS applied materials & interfaces. 2014;6(16):13688-96.

[13] Roul MK, Beckford J, Obasogie B, Yarbrough K, Bahoura M, Pradhan A. High-performance transparent film heater using random mesowire silver network. Journal of Materials Science: Materials in Electronics. 2018;29(24):21088-96.

[14] Kiruthika S, Gupta R, Kulkarni GU. Large area defrosting windows based on electrothermal heating of highly conducting and transmitting Ag wire mesh. Rsc Advances. 2014;4(91):49745-51.

[15] Kiruthika S, Rao K, Kumar A, Gupta R, Kulkarni G. Metal wire network based transparent conducting electrodes fabricated using interconnected crackled layer as template. Materials Research Express. 2014;1(2):026301.

[16] Gupta R, Kumar A, Sadasivam S, Walia S, Kulkarni GU, Fisher TS, et al. Microscopic evaluation of electrical and thermal conduction in random metal wire networks. ACS applied materials & interfaces. 2017;9(15):13703-12.

[17] Rao K, Kulkarni GU. A highly crystalline single Au wire network as a high temperature transparent heater. Nanoscale. 2014;6(11):5645-51.

[18] Huang X, Zhang F, Leng J. Metal mesh embedded in colorless shape memory polyimide for flexible transparent electric-heater and actuators. Applied Materials Today. 2020;21:100797.

[19] Zhao L, Yu S, Li X, Wu M, Li L. High-performance copper mesh transparent flexible conductors based on electroplating with vacuum-free processing. Organic Electronics. 2020;82:105511.

[20] Chen T, Li H, Li J, Hu S, Ye P, Yan Y. Direct writing of silver microfiber with precise control on patterning for robust and flexible ultrahigh-performance transparent conductor. Journal of Materials Science & Technology. 2020;47:103-12.
[21] Gupta R, Walia S, Hösel M, Jensen J, Angmo D, Krebs FC, et al. Solution processed large area fabrication of Ag patterns as electrodes for flexible heaters, electrochromics and organic solar cells. Journal of Materials Chemistry A. 2014;2(28):10930-7.
[22] Seong B, Yoo H, Nguyen VD, Jang Y, Ryu C, Byun D. Metal-mesh based transparent electrode on a 3-D curved surface by electrohydrodynamic jet printing. Journal of Micromechanics and Microengineering. 2014;24(9):097002.
[23] Thouti E, Mistry C, Chandran A, Panwar DK, Kumar P, Suman H, et al. Study of seamless Au mesh flexible transparent heaters: Influence of mesh coverage. Journal of Physics D: Applied Physics. 2019;52(42):425301.
[24] Bobinger M, Mock J, La Torraca P, Becherer M, Lugli P, Larcher L. Tailoring the aqueous synthesis and deposition of copper nanowires for transparent electrodes and heaters. Advanced Materials Interfaces. 2017;4(20):1700568.
[25] Bobinger M, La Torraca P, Mock J, Becherer M, Cattani L, Angeli D, et al. Solution-processing of copper nanowires for transparent heaters and thermo-acoustic loudspeakers. IEEE Transactions on Nanotechnology. 2018;17(5):940-7.
[26] Das SR, Mohammed AM, Maize K, Sadeque S, Shakouri A, Janes DB, et al. Evidence of universal temperature scaling in self-heated percolating networks. Nano letters. 2016;16(5):3130-6.
[27] Gupta MP, Kumar N, Kumar S. Computational Study of Thermal Transport in Nanowire-Graphene Thin Films. IEEE Transactions on Nanotechnology. 2018;17(4):829-36.
[28] Rocha CG, Manning HG, O'Callaghan C, Ritter C, Bellew AT, Boland JJ, et al. Ultimate conductivity performance in metallic nanowire networks. Nanoscale. 2015;7(30):13011-6.
[29] O'Callaghan C, Rocha CG, Manning HG, Boland JJ, Ferreira MS. Effective medium theory for the conductivity of disordered metallic nanowire networks. Physical Chemistry Chemical Physics. 2016;18(39):27564-71.
[30] Kumar A, Kulkarni G. Evaluating conducting network based transparent electrodes from geometrical considerations. Journal of Applied Physics. 2016;119(1):015102.